








# Comprehensive model for ideal reverse leakage current components in Schottky barrier diodes tested in GaN-on-SiC samples

Cite as: J. Appl. Phys. **132**, 044502 (2022); doi: [10.1063/5.0100426](https://doi.org/10.1063/5.0100426)

Submitted: 24 May 2022 · Accepted: 1 July 2022 ·

Published Online: 25 July 2022



B. Orfao,<sup>1,a)</sup>  G. Di Gioia,<sup>2</sup>  B. G. Vasallo,<sup>1</sup>  S. Pérez,<sup>1</sup>  J. Mateos,<sup>1</sup>  Y. Roelens,<sup>2</sup> E. Frayssinet,<sup>3</sup> Y. Cordier,<sup>3</sup>   
M. Zaknoute,<sup>2</sup> and T. González<sup>1</sup> 

## AFFILIATIONS

<sup>1</sup>Dpto. Física Aplicada and USAL-NANOLAB, Universidad de Salamanca, 37008 Salamanca, Spain

<sup>2</sup>CNRS-IEMN, Université de Lille, UMR8520, Av. Poincaré, 59650 Villeneuve d'Ascq, France

<sup>3</sup>Université Côte d'Azur, CNRS, CRHEA, rue B. Grégory, 06560 Valbonne, France

<sup>a)</sup>Author to whom correspondence should be addressed: [beatrizorfao@usal.es](mailto:beatrizorfao@usal.es)

## ABSTRACT

A model to predict the ideal reverse leakage currents in Schottky barrier diodes, namely, thermionic emission and tunneling components, has been developed and tested by means of current–voltage–temperature measurements in GaN-on-SiC devices. The model addresses both current components and both forward and reverse polarities in a unified way and with the same set of parameters. The values of the main parameters (barrier height, series resistance, and ideality factor) are extracted from the fitting of the forward-bias  $I$ - $V$  curves and then used to predict the reverse-bias behavior without any further adjustment. An excellent agreement with the  $I$ - $V$  curves measured in the forward bias in the GaN diode under analysis has been achieved in a wide range of temperatures (275–475 K). In reverse bias, at temperatures higher than 425 K, a quasi-ideal behavior is found, but additional mechanisms (most likely trap-assisted tunneling) lead to an excess of leakage current at lower temperatures. We demonstrate the importance of the inclusion of image-charge effects in the model in order to correctly predict the values of the reverse leakage current. Relevant physical information, like the energy range at which most of the tunnel injection takes place or the distance from the interface at which tunneled electrons emerge, is also provided by the model.

Published under an exclusive license by AIP Publishing. <https://doi.org/10.1063/5.0100426>

## I. INTRODUCTION

Schottky barrier diodes (SBDs) have demonstrated excellent high-frequency performance which has allowed the fabrication of RF sources reaching the THz range<sup>1</sup> or building sensitive direct detectors of THz radiation at room temperature.<sup>2,3</sup> In the past few years, wide-bandgap semiconductors like SiC and GaN have started to be used for the fabrication of SBDs oriented to high-power applications, which have today a broad field of purposes like the production of on-board battery chargers and off-board charging stations for the electric vehicle industry,<sup>4,5</sup> DC/DC boost converters, DC/AC inverters for solar and renewable energy applications,<sup>6</sup> etc.

GaN-based devices have already demonstrated good performances for high-power, high-frequency, and high-temperature electronics, mainly using the classical High Electron Mobility Transistor (HEMT) technology.<sup>7</sup> GaN SBDs are also believed to be

suitable for the next generation of high-power circuits.<sup>8</sup> They could offer high switching speed and low reverse recovery loss in switched-mode power supplies, thus competing with SiC SBD technology as well as challenge the power handling capabilities of the standard GaAs technology used in sub-THz multipliers.<sup>9</sup> However, issues related to defects that originate a high reverse leakage current, degrading their breakdown voltage and reliability, have hindered the use of GaN SBDs for practical applications.<sup>10</sup> The modeling of carrier transport through the metal–semiconductor rectifying contact is essential to identify the origin of the technological problems and find solutions for the exploitation of GaN SBDs in modern electronic applications. Additionally, the in-depth knowledge of these contacts is essential in understanding other semiconductor devices, like field-effect transistors, where they act as a gate terminal, controlling the electrical performance of devices.

The dominant current mechanism in the forward-bias current of SBDs is thermionic emission over the energy barrier formed at the metal–semiconductor interface.<sup>11</sup> However, the electrical properties of fabricated devices deviate from the fundamental theory, and additional fitting parameters like the ideality factor and the series resistance are necessary to correctly reproduce the experimental  $I$ – $V$  curves.<sup>12–14</sup> In the reverse bias, ideally, in addition to thermionic emission, tunneling current becomes important.<sup>13</sup> This leakage current contribution affects the high-power operation of SBDs and degrades their breakdown characteristics.<sup>15</sup> The widely accepted models by Murphy and Good<sup>16</sup> and Padovani and Stratton<sup>17</sup> provide analytical expressions for the current only applicable in some specific ranges of the reverse bias. Here, one of the difficulties is the inclusion of image-charge (IC) effects, with the associated barrier lowering, necessary to determine precisely the reverse current at low values of the surface electric field, when the shape of the barrier top is of importance. Analytical expressions by means of a trapezoidal approximation for the barrier have been derived in the literature.<sup>18,19</sup>

However, deviations from these two (thermionic-emission and tunneling) ideal current components are regularly observed in the reverse bias. In some cases, mainly in non-mature technologies, current values much higher than expected are measured, leading to a premature breakdown of the devices.<sup>20</sup> The (non-ideal) additional contributions to the reverse leakage current can be due to interface or deep-level defects and dislocations. These effects can be especially important in GaN SBDs and related wide-bandgap devices because of their relatively high defect density.<sup>10</sup> Mechanisms such as trap-assisted tunneling, Poole–Frenkel emission or

variable-range hopping have been typically identified as sources of leakage current in GaN SBDs.<sup>15,20–22</sup> Enhanced performance has been achieved by appropriate growing conditions,<sup>23</sup> surface treatments,<sup>24</sup> or contact terminations.<sup>15,25</sup>

In order to assess how ideal is the behavior of SBDs in the reverse bias and evaluate correctly the excess current contributions associated with other leakage mechanisms, the development of an accurate model for thermionic emission and tunneling currents is essential. Such a model should be consistent with the behavior of the diode in the forward bias, this is, described by the same parameters in both polarities, which requires to address them simultaneously.<sup>18,26</sup> In this work, we develop a comprehensive unified model for thermionic and tunneling currents describing transport in both polarities with a single set of physically meaningful parameters, determined from the fitting of the  $I$ – $V$  curve in the forward bias and then applied to predict the diode behavior in the reverse bias (with no other adjustable factors). The model includes a detailed numerical treatment of IC, shown to be necessary to reproduce experimental results, and the influence of the epilayer doping in the shape of the barrier. Current–voltage–temperature characteristics measured in GaN-on-SiC SBDs fabricated at IEMN<sup>27</sup> have been used to validate the model, thereby finding always excellent agreement in the forward bias and also for the highest temperatures in the reverse bias, thus corroborating the good quality of the technological process used. For temperatures below 400 K, leakage current in excess is observed and attributed to trap-assisted tunneling.

The paper is organized as follows. The model is described in Sec. II. Experimental details about the devices and measurements are reported in Sec. III. The results and their discussion are provided in Sec. IV. Finally, the main conclusions are drawn in Sec. V.

## II. MODEL

The total current in an ideal SBD is formed of two components: thermionic emission,  $J_{th}$ , and tunneling,  $J_{tunnel}$ . In the forward bias, as long as the Schottky layer is moderately doped, the current is essentially due to thermionic emission, and  $J_{tunnel}$  can be neglected; while in the reverse bias, depending on the applied voltage  $V$ , both contributions may be of importance. Thus, in our model, we will consider the current components shown in Fig. 1, corresponding to the thermionic emission of electrons from the semiconductor to the metal  $J_{th}^{s \rightarrow m}$ , from the metal to the semiconductor  $J_{th}^{m \rightarrow s}$ , and to the tunneling of electrons from the metal to the semiconductor  $J_{tunnel}^{m \rightarrow s}$ .

The values of these current components for a given  $V$  depend on the height and shape of the energy barrier. Taking the metal Fermi level  $\epsilon_{Fm}$  as the zero-energy reference, and including the influence of the IC and the doping of the active layer  $N_D$ , the potential energy in the Schottky layer at a distance  $x$  from the metal interface is given by<sup>28,29</sup>

$$\epsilon_C(x) = e\phi_B - e \left[ \frac{2eN_D}{\epsilon_s} (V_B - V) \right]^{\frac{1}{2}} x + \frac{e^2 N_D x^2}{2\epsilon_s} - \frac{e^2}{16\pi\epsilon_s x}, \quad (1)$$

where  $\phi_B$  is the barrier height,  $V_B$  the built-in potential, and  $\epsilon_s$  the permittivity of the semiconductor. Note that the second term

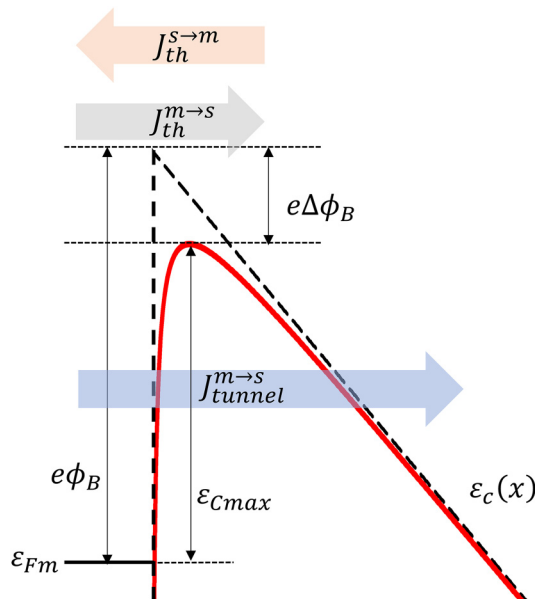


**FIG. 1.** Scheme of the energy barrier with and without IC corrections, and current contributions considered in the model. The arrows indicate the movement of electrons, currents flow in the opposite sense.

in Eq. (1) corresponds to  $-eEx$ , with  $E$  being the surface electric field at the metal–semiconductor interface, and the third term accounts for the influence of the doping and the last one for the lowering of the barrier due to the IC.

We will use a general formalism for the calculation of these current components. The injected current from one side of the junction into the other one in the range  $d\epsilon$  around an energy  $\epsilon$  normal to the barrier can be written as

$$J(\epsilon)d\epsilon = -eN(\epsilon)T_C(\epsilon)d\epsilon, \quad (2)$$

where

$$N(\epsilon) = \frac{A^*T}{ek_B} \ln \left[ 1 + \exp \left( -\frac{\epsilon - \epsilon_F}{k_B T} \right) \right] \quad (3)$$

is the number of electrons per unit area incident on the barrier with normal energy  $\epsilon$  per unit time and per unit energy<sup>30</sup> at the side (metals or semiconductors) from which they are injected and  $T_C(\epsilon)$  is the transmission coefficient corresponding to that energy.  $\epsilon_F$  is the Fermi energy at the side (metals or semiconductors) from which electrons are injected,  $T$  the absolute temperature and  $A^* = 4\pi m^* k_B^2 e / h^3$  the effective Richardson constant, with  $k_B$  being the Boltzmann constant,  $m^*$  the electron effective mass of the semiconductor, and  $h$  the Planck constant. We will consider a single effective mass for both the Richardson constant and the tunneling effective mass.<sup>18,28</sup> Equation (2) assumes a negligible occupation of the states with energy  $\epsilon$  at the side into which electrons are injected, as expected for the case of thermionic contributions (as long as the barrier is high enough) and tunneling from the metal to the semiconductor in the reverse bias.

$T_C(\epsilon) = 1$  for energies above the maximum of the barrier  $\epsilon > \epsilon_{Cmax}$ , corresponding to thermionic-emission processes, while for  $\epsilon < \epsilon_{Cmax}$ , corresponding to tunneling processes,  $T_C(\epsilon)$  is calculated using the Wentzel–Kramers–Brillouin (WKB) approximation for the evaluation of the tunneling probability as<sup>31</sup>

$$T_C(\epsilon) = \exp \left[ -\frac{2}{\hbar} \int_{x_1}^{x_2} \sqrt{2m^*(\epsilon_c(x) - \epsilon)} dx \right], \quad (4)$$

with  $x_1$  and  $x_2$  being the classical turning points at which  $\epsilon_c(x) = \epsilon$ .

As shown in Fig. 1,  $\epsilon_{Cmax} = e(\phi_B - \Delta\phi)$ , where  $\Delta\phi = \sqrt{eE/4\pi\epsilon_s}$  is the IC lowering of the barrier [calculated neglecting the influence of  $N_D$ , third term in Eq. (1)]. If IC effects are neglected,  $\epsilon_{Cmax} = e\phi_B$ .

Thus, the current associated with electrons injected from the metal to the semiconductor is calculated as<sup>28</sup>

$$\begin{aligned} J^{m \rightarrow s} &= -e \int_{\epsilon_{min}}^{\infty} N_m(\epsilon) T_C(\epsilon) d\epsilon \\ &= -e \int_{\epsilon_{min}}^{\epsilon_{Cmax}} N_m(\epsilon) T_C(\epsilon) d\epsilon - e \int_{\epsilon_{Cmax}}^{\infty} N_m(\epsilon) d\epsilon \\ &= J_{tunnel}^{m \rightarrow s} + J_{th}^{m \rightarrow s}, \end{aligned} \quad (5)$$

where  $\epsilon_{min}$  is the minimum energy in the metal for which tunneling into the semiconductor is possible (there must be available states in the conduction band of the semiconductor at the same energy). For the sake of accuracy, the calculation of  $J_{tunnel}^{m \rightarrow s}$  is performed numerically, since there is no simple analytical expression for  $T_C(\epsilon)$  when IC corrections are included in the energy barrier, despite trapezoidal approximations have been reported.<sup>18,19</sup> In the case of  $J_{th}^{m \rightarrow s}$ , since the involved energies typically fulfill  $\epsilon - \epsilon_{Fm} \gg k_B T$ , it is possible to approximate

$$N_m(\epsilon) \approx \frac{A^*T}{ek_B} \exp \left( -\frac{\epsilon - \epsilon_{Fm}}{k_B T} \right), \quad (6)$$

thereby allowing to evaluate  $J_{th}^{m \rightarrow s}$  analytically as

$$J_{th}^{m \rightarrow s} = -A^* T^2 \exp \left( -\frac{\epsilon_{Cmax}}{k_B T} \right). \quad (7)$$

As explained before, the current associated with electrons injected from the semiconductor to the metal is considered to be only due to thermionic emission. Assuming no collision of electrons in the depletion region (coherent with the relatively high mobility of GaN in our case), this current is given by

$$J^{s \rightarrow m} = J_{th}^{s \rightarrow m} = e \int_{\epsilon_{Cmax}}^{\infty} N_s(\epsilon) d\epsilon. \quad (8)$$

Again, since the involved energies typically fulfill  $\epsilon - \epsilon_{Fs} \gg k_B T$ , it is possible to approximate

$$N_s(\epsilon) \approx \frac{A^*T}{ek_B} \exp \left( -\frac{\epsilon - \epsilon_{Fs}}{k_B T} \right). \quad (9)$$

Taking into account that  $\epsilon_{Fs} = \epsilon_{Fm} + eV$ , one arrives to

$$J_{th}^{s \rightarrow m} = A^* T^2 \exp \left( -\frac{\epsilon_{Cmax}}{k_B T} \right) \exp \left( \frac{eV}{k_B T} \right). \quad (10)$$

The total thermionic emission current will thus be given by

$$\begin{aligned} J_{th} &= J_{th}^{s \rightarrow m} + J_{th}^{m \rightarrow s} = A^* T^2 \exp \left( -\frac{\epsilon_{Cmax}}{k_B T} \right) \left[ \exp \left( \frac{eV}{k_B T} \right) - 1 \right] \\ &= J_0 \left[ \exp \left( \frac{eV}{k_B T} \right) - 1 \right]. \end{aligned} \quad (11)$$

In a general case with IC effects included, the reverse saturation current  $J_0$  is  $A^* T^2 \exp[-e(\phi_B - \Delta\phi_B)/k_B T]$  and thus depends on the applied voltage  $V$  through  $\Delta\phi_B$ .

This ideal expression for  $J_{th}$  must be further modified to include real effects, like the influence of the series resistance  $R_s$  and the ideality factor  $\eta$ , as

$$J_{th}(V) = J_0 \left[ e^{\frac{e(V - J_{th} R_s)}{\eta k_B T}} - 1 \right], \quad (12)$$

where  $S$  is the surface of the Schottky contact. The inclusion of

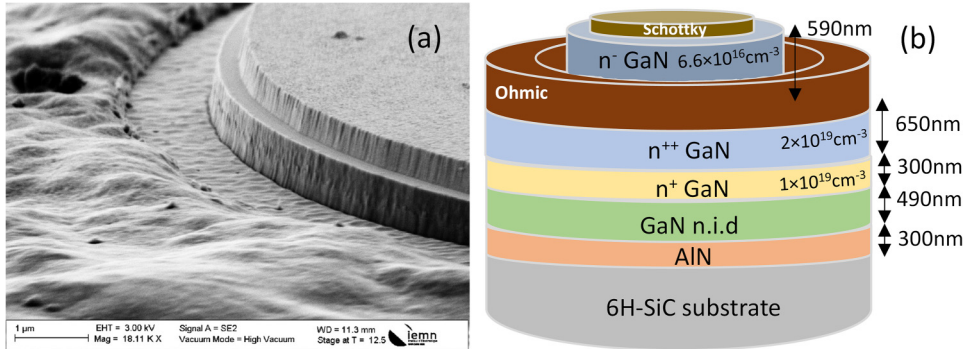


**FIG. 2.** (a) SEM image of a real SBD fabricated at the IEMN and (b) scheme of the epitaxial layer.

these two parameters, external to the ideal model, is necessary to achieve a good fitting of the forward  $I$ - $V$  curves, essential to accurately determine  $\phi_B$ .

The final aim of this model is to predict the ideal reverse  $I$ - $V$  characteristics of SBDs as a function of temperature  $T$ . Six parameters are involved in the model, namely,  $\phi_B$ ,  $N_D$ ,  $\epsilon_s$ ,  $m^*$ ,  $R_s$ , and  $\eta$ . We proceed as follows to determine their values.  $\epsilon_s$  and  $m^*$  are taken from the literature:  $8.9\epsilon_0$  and  $0.22 m_0$  (giving  $A^* = 26.4 \text{ A cm}^{-2} \text{ K}^{-2}$ ) for the case of GaN. We use the low-frequency permittivity for both the surface electric field and the IC term. The value of  $N_D$  is extracted from  $C$ - $V$  measurements in the reverse bias ( $1.05 \times 10^{17} \text{ cm}^{-3}$  in our case). And finally,  $\phi_B$ ,  $R_s$ , and  $\eta$  are determined from the fitting to Eq. (12) of the experimental  $I$ - $V$  curves measured in the forward bias.

Once the values of the parameters are determined, they are used to predict the reverse  $I$ - $V$  characteristics, including thermionic and tunneling currents, as

$$J_{\text{reverse}}(V) = J_{\text{th}}(V) + J_{\text{tunnel}}^{m \rightarrow s}(V), \quad (13)$$

without any further fitting or adjustment of parameters.

In order to confirm the need to include the IC correction in the calculations, a fitting of the  $I$ - $V$  curve measured in the forward bias will also be performed without considering the influence of IC, thus obtaining an effective barrier height  $\phi_B^{\text{eff}}$ , lower than the value of  $\phi_B$  extracted when IC is considered, and the corresponding  $\eta^{\text{eff}}$ . Remarkably, excellent agreement of the forward  $I$ - $V$  curves can be attained in both ways, which could erroneously lead us to believe that the reverse  $I$ - $V$  curve should also be well predicted by both approaches. To check this fact, calculations of the reverse  $I$ - $V$  characteristics with the full model [including IC and taking  $\mathcal{E}_{C\text{max}} = e(\phi_B - \Delta\phi)$ ] will be compared with those ignoring IC [removing the last term in Eq. (11)] and using effective parameters ( $\mathcal{E}_{C\text{max}} = e\phi_B^{\text{eff}}$ ) to eventually determine which is the model best fitting the experimental reverse  $I$ - $V$  curves.

### III. EXPERIMENTAL

GaN-on-SiC SBDs fabricated at IEMN have been characterized to validate the model.<sup>27</sup> The epitaxial layer was grown at CRHEA by metal organic vapor phase epitaxy on a semi-insulating 6H-SiC substrate. A SEM image of one of the diodes is shown in

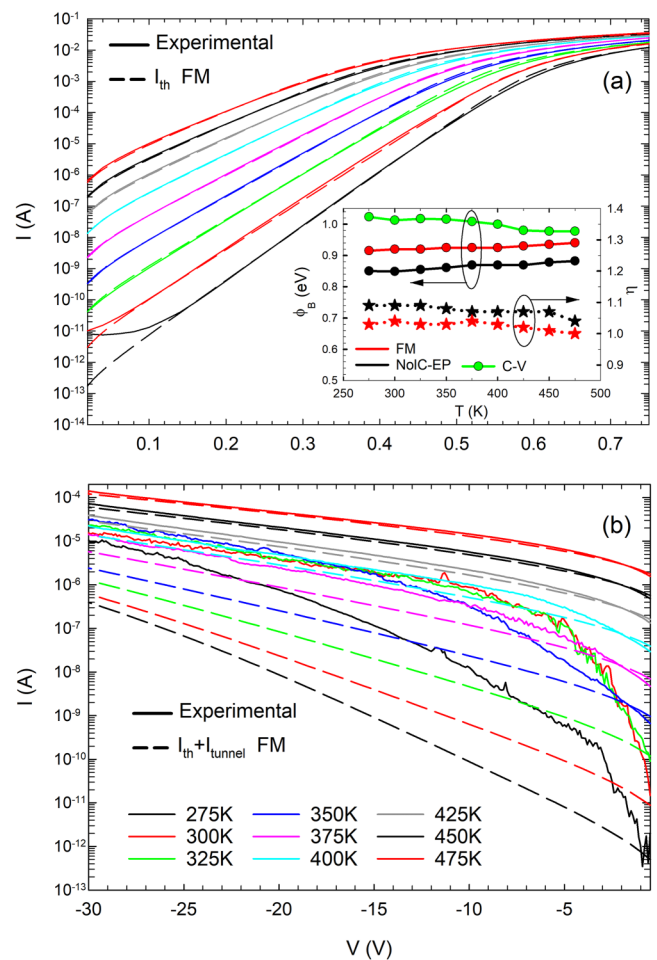


**FIG. 3.** Measured (solid lines) and modeled (dashed lines)  $I$ - $V$  curves for (a) forward and (b) reverse bias. The (full) model includes thermionic emission and tunneling currents (the latter only in the reverse bias) with the influence of IC and  $R_s$ . Inset:  $\phi_B$  and  $\eta$  extracted by fitting the full model (FM) to the experimental curves in the forward bias; the values of the effective parameters  $\phi_B^{\text{eff}}$  and  $\eta^{\text{eff}}$  fitting the forward  $I$ - $V$  curves in the absence of IC effects (NoIC-EP case) and the barrier height extracted from the  $C$ - $V$  curves are also shown.



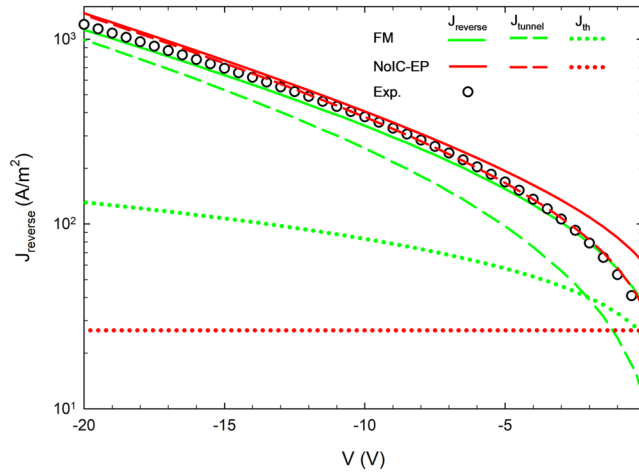


**FIG. 4.** Current density in the reverse bias modeled including IC (FM, green lines) and without IC using effective parameters (NoIC-EP, red lines) as compared to measurements (circles). For the modeled values, the two ideal contributions, tunneling current (dashed lines) and thermionic emission (dotted lines), as well as the total reverse value (solid lines), are represented.  $T = 475$  K.

Fig. 2(a), while the details of the epitaxial layer are provided in the scheme of Fig. 2(b). A 490 nm unintentionally doped GaN was grown first, followed by a highly doped 950 nm thick GaN layer (300 nm @  $1 \times 10^{19} \text{ cm}^{-3}$  and 650 nm @  $2 \times 10^{19} \text{ cm}^{-3}$ ) to achieve a good ohmic contact and a low series resistance, and finally a 1  $\mu\text{m}$   $n^-$  GaN layer (nominally  $6.6 \times 10^{16} \text{ cm}^{-3}$ ) acting as the Schottky layer. The diode mesa definition was made by  $\text{Cl}_2/\text{Ar}$  ICP dry etch using a 250 nm thick PECVD  $\text{SiO}_2$  hard mask. After the diode mesa etching, the  $\text{SiO}_2$  hard mask is left on the top of the Schottky core in order to protect the surface from damage and contamination during the subsequent technological steps. Then, just after a Buffered Oxide Etch (BOE) surface cleaning, a standard Ti/Al/Ni/Au ohmic contact was deposited on the  $n^{++}$  layer with an e-beam metal evaporator. Next, a rapid thermal annealing was performed at 850  $^\circ\text{C}$  for 30 s in a  $\text{N}_2$  ambient. Before the Schottky contact deposition, the sample was treated again with a BOE solution to remove the remaining  $\text{SiO}_2$  layer and thus uncover the GaN epilayer surface. Apart from removing the  $\text{SiO}_2$  hard mask, BOE acts as surface treatment by eliminating the evaporants and oxidized GaN. Hereafter, a rapid introduction in the evaporator is performed in order to avoid surface re-oxidation and Pt/Au metals are deposited on the top  $n^-$  layer. The results shown in this work correspond to a circular diode with a diameter of 221  $\mu\text{m}$ . The large area of the Schottky contact allows expecting a negligible influence of edge effects. Diodes with other similar sizes exhibit the same qualitative behavior.

$I$ - $V$  and  $C$ - $V$  measurements have been performed at different temperatures by means of a LakeShore CRX-VF cryogenic probe station. Assuming an ionization energy of 15 meV for Si donors in GaN,<sup>32</sup> the fraction of ionized atoms (for the nominal doping of the epilayer) should theoretically increase from 90% to 96% in the analyzed temperature range (275–450 K). However, the  $C$ - $V$  measurements in the reverse bias used to extract the doping of the

epilayer  $N_D$  provide a temperature-independent value of about  $1.05 \times 10^{17} \text{ cm}^{-3}$ , which will be the one used in the calculations. Barrier height values are also extracted from  $C$ - $V$  measurements but, for consistency, we will adopt the values fitting the forward  $I$ - $V$  characteristics.

#### IV. RESULTS AND DISCUSSION

Current-voltage-temperature measurements were carried out from 275 to 475 K, as shown in Fig. 3 for (a) forward and (b) reverse bias. Note that the lower limit of the measurements is about  $10^{-11}$  A. The expected increase of current with temperature is observed. As explained, the ideal model for the forward  $I$ - $V$  characteristics includes the thermionic emission contribution  $J_{th}$  incorporating the lowering of the barrier originated by IC. Additionally, real effects like the influence of the series resistance  $R_s$  and the ideality factor  $\eta$  are accounted for to provide the final expression given by Eq. (12). As observed in Fig. 3(a), our model reproduces very closely the experimental curves. From the fitting, the values of  $\phi_B$ ,  $\eta$ , and  $R_s$  at each temperature are determined, obtaining very reasonable values well within the range of those in the literature.<sup>12,13,33</sup>

The inclusion of  $R_s$ , taking values around 10  $\Omega$  for all the temperatures, is essential to fit the experimental values for current levels above  $10^{-4}$  A. Since the resistances associated with the epilayer, substrate, and ohmic contact are of the order of tenths of  $\Omega$  for the diode size used here, this value of  $R_s$  corresponds essentially to the contribution of the cables and probes used in our setup, which are expected to be nearly temperature independent. The values of  $\phi_B$  and  $\eta$  extracted from the fittings are provided in the inset as a function of temperature. Values of  $\phi_B$  in the range of 0.92–0.94 eV are obtained, while the ideality factor is always lower than 1.05 (nearly 1 for the highest temperatures), indicating the good quality of the diodes. The slight increase of  $\phi_B$  and decrease of  $\eta$  with growing  $T$  evidence a small influence of inhomogeneities.<sup>26</sup>

Once the parameters of the model have been fixed from the fitting of the forward  $I$ - $V$  curves, we can use it to predict the ideal behavior of the diodes in the reverse bias, where, in addition to the thermionic current, the tunnel contribution, calculated as indicated in Eq. (5), is also included. As observed in Fig. 3(b), for the highest temperatures, the results of the model practically coincide with the experimental values, thus confirming the validity of our approach and the nearly ideal behavior of the diodes. However, for temperatures below 425 K, the current values deviate from the addition of the two ideal contributions, exhibiting significantly higher values, which means that additional non-ideal leakage current mechanisms are present.

An excellent fitting (not shown) of the forward  $I$ - $V$  curves, similar to that reported in Fig. 3(a), can also be obtained if IC effects are ignored in the model and different values of the barrier height and ideality factor are used,  $\phi_B^{\text{eff}}$  and  $\eta^{\text{eff}}$ , respectively, denoted as effective parameters [also shown in the inset of Fig. 3(a) as the NoIC-EP case]. As expected,  $\phi_B^{\text{eff}}$  is systematically lower than  $\phi_B$  to afford the same current level in the absence of IC barrier lowering. On the other hand,  $\eta^{\text{eff}}$  lies in the range of 1.05–1.10, thus exhibiting a slightly higher deviation from ideality than when IC is considered. Finally, the barrier height obtained from the  $C$ - $V$  curves is also plotted for comparison in the inset. The values are higher than those

obtained from the  $I$ - $V$  curves, as often observed in several technologies,<sup>12,13</sup> including GaN,<sup>33</sup> and typically attributed to non-ideal interfaces (inhomogeneities, interfacial charges, etc.).<sup>12</sup>

Despite the excellent agreement obtained in the forward bias by both the full model (denoted as FM) and the case ignoring IC effects but using effective parameters (denoted as NoIC-EP), in Fig. 4 we show that only the former is able to correctly predict the behavior of the diode in the reverse bias, especially for low voltages. To compare both approaches, we have performed calculations at 475 K, where we have already confirmed that the behavior of the

diode is practically ideal, and the FM is able to correctly reproduce the experimental results. In the figure, the measured values are compared with the total reverse current ( $J_{reverse}$ ) obtained in both cases. The thermionic ( $J_{th}$ ) and tunnel ( $J_{tunnel}$ ) contributions are also shown for completeness. In the absence of IC, the NoIC-EP case provides the expected bias-independent  $J_{th}$ , which is practically negligible as compared to  $J_{tunnel}$  in all the bias range. In the case of the FM,  $J_{th}$ , apart from being larger due to the barrier lowering, increases with the reverse bias as corresponds to the higher surface electric field. On the other hand,  $J_{th}$  is comparable or even higher

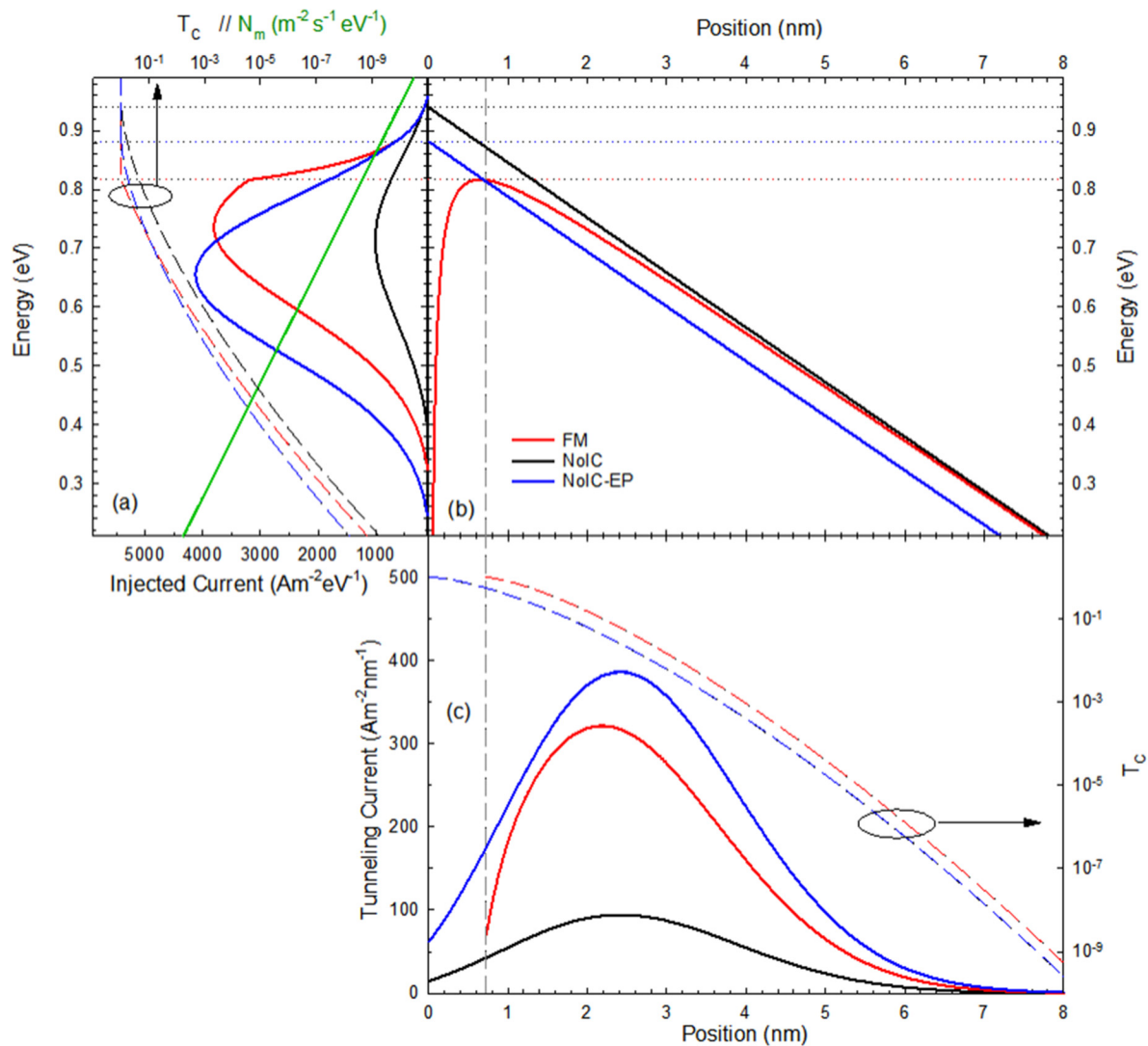


**FIG. 5.** Comparison of three case studies for  $T = 475$  K and  $V = -20$  V: (i) including IC (FM, red lines), (ii) without IC and using the same parameters as the FM (NoIC, black lines) and (iii) without IC but using the effective parameters (NoIC-EP, blue lines). (a) Injected current (solid lines), transmission coefficient (dashed lines), and rate of electrons incident on the barrier [Eq. (6), green line] as a function of energy; (b) conduction band and (c) tunneling current (solid lines) and transmission coefficient (dashed lines) as a function of the distance from the metal-semiconductor interface. The horizontal dotted lines in (a) and (b) indicate the top of the barrier in each case, i.e., the energy separating tunneling and thermionic injection. The vertical dashed line in (b) and (c) indicates the position of the maximum of the barrier in the FM case.

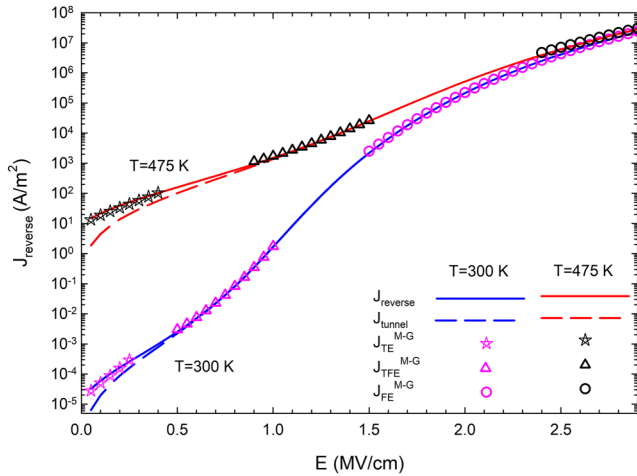


**FIG. 6.** Current density as a function of the surface electric field obtained by means of our numerical model (solid lines, total current; dashed lines, tunneling current) and by Murphy and Good's analytical model (symbols) for two temperatures,  $T = 300$  K (blue) and  $T = 475$  K (red). Murphy and Good's results are represented in the range of validity corresponding to the different current regimes: thermionic emission (TE, stars), thermionic field emission (TFE, triangles) and field emission (FE, circles).

than  $J_{tunnel}$  at lower voltages. As concerns  $J_{tunnel}$ , it is substantially higher in the NoIC-EP case, mainly at the lower values of the reverse bias, due to the thinner energy barrier [see Fig. 5(b)]. The relative difference diminishes when the bias increases since a significant electron injection takes place at (lower) energies not so close to the top of the barrier. As a result of these differences, the total current is overestimated in the NoIC-EP case, mainly at the lowest voltages. We conclude that the FM, including the IC correction, is necessary to correctly reproduce the current in the reverse bias.

In order to understand the key role played by the barrier lowering associated with IC effects, and exploiting the capabilities of the model to provide a deep physical insight of injection processes in the reverse bias, in Fig. 5 we compare, for a temperature of 475 K and a bias of  $-20$  V, the details of electron injection as a function of energy and position in three case studies: (i) including IC effects (FM case), (ii) without including IC effects and using the same parameters as the FM (NoIC case), and (iii) without including IC effects but using the effective parameters (NoIC-EP case). While cases (i) and (iii) provide similar values of the total reverse current ( $1.12 \times 10^3$  and  $1.38 \times 10^3$  A/m<sup>2</sup>, respectively, see Fig. 4), case (ii), by considering a too high barrier, obviously underestimates the current ( $0.34 \times 10^3$  A/m<sup>2</sup>).

Figure 5(b) shows the shape of the conduction band in each of the cases. At this temperature,  $e\phi_B = 0.940$  eV and  $e\phi_B^{eff} = 0.882$  eV, and for a bias of  $-20$  V,  $e\Delta\phi_B = 0.123$  eV. Thus, the maximum of the barrier  $\epsilon_{Cmax}$  in the FM case is  $e(\phi_B - \Delta\phi_B) = 0.817$  eV. As expected,  $e\phi_B^{eff}$  takes an intermediate value between  $e\phi_B$  and  $e(\phi_B - \Delta\phi_B)$ . Figure 5(a) shows the current injected per unit energy  $J(\epsilon)$ , jointly with the transmission coefficient  $T_C(\epsilon)$  and the rate of incident electrons  $N_m(\epsilon)$ .  $T_C = 1$  once the energy is higher than

$\epsilon_{Cmax}$ , corresponding to the range of thermionic emission, where, as expected,  $J(\epsilon)$  coincides in the three cases. For this bias, tunnel injection takes place mainly at energies fulfilling  $\epsilon - \epsilon_{Fm} \gg k_B T$ , so that  $N_m(\epsilon)$  exhibits the exponential behavior described by Eq. (6). It is remarkable that the average energy of the tunneled electrons is higher within the FM, fact that may have important implications for the precise calculation of the breakdown voltage (higher energies lead to earlier impact-ionization and avalanche). Finally, in Fig. 5(c), the transmission coefficient and the tunneling current per unit length are represented as a function of the distance to the metal-semiconductor interface. The transmission coefficient of the two cases without IC is exactly the same since the barrier seen by carriers injected at a given position is identical in both cases. As observed, for this applied voltage, tunnel injection takes place mainly along the first 5–6 nm from the interface, slightly closer to the metal when IC is considered.

Another test for the correctness of our model is the comparison with existing analytical models whose validity is restricted to some ranges of surface electric field values, like those of Murphy and Good<sup>16</sup> and Padovani and Stratton.<sup>17</sup> None of the mentioned models correspond exactly to our FM, since Padovani and Stratton ignore IC effects (thus, their model corresponds to our NoIC-EP case) and Murphy and Good ignore the effect of the doping [third term in the right-hand side of Eq. (1)]. Our model, considering the appropriate terms, correctly reproduces the results of both models, as shown in Fig. 6 for the case of Murphy and Good's model at 300 and 475 K. We represent both the total and the tunneling current calculated by our model excluding the influence of the doping (which, on the other hand, could be significant for highly doped SBDs oriented to ultra-high-frequency applications). For the lower values of the electric field, Murphy and Good's thermionic emission current ( $J_{TE}^{M-G}$ ), which, despite the name, includes also the tunneling contribution, is well reproduced by the total current

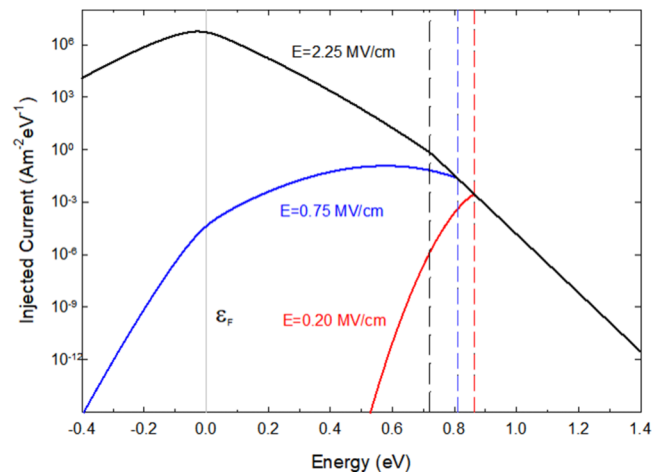


**FIG. 7.** Injected current as a function of energy for three different surface electric fields at 300 K. Vertical lines indicate the Fermi level and the energy corresponding to the top of the barrier in each case.

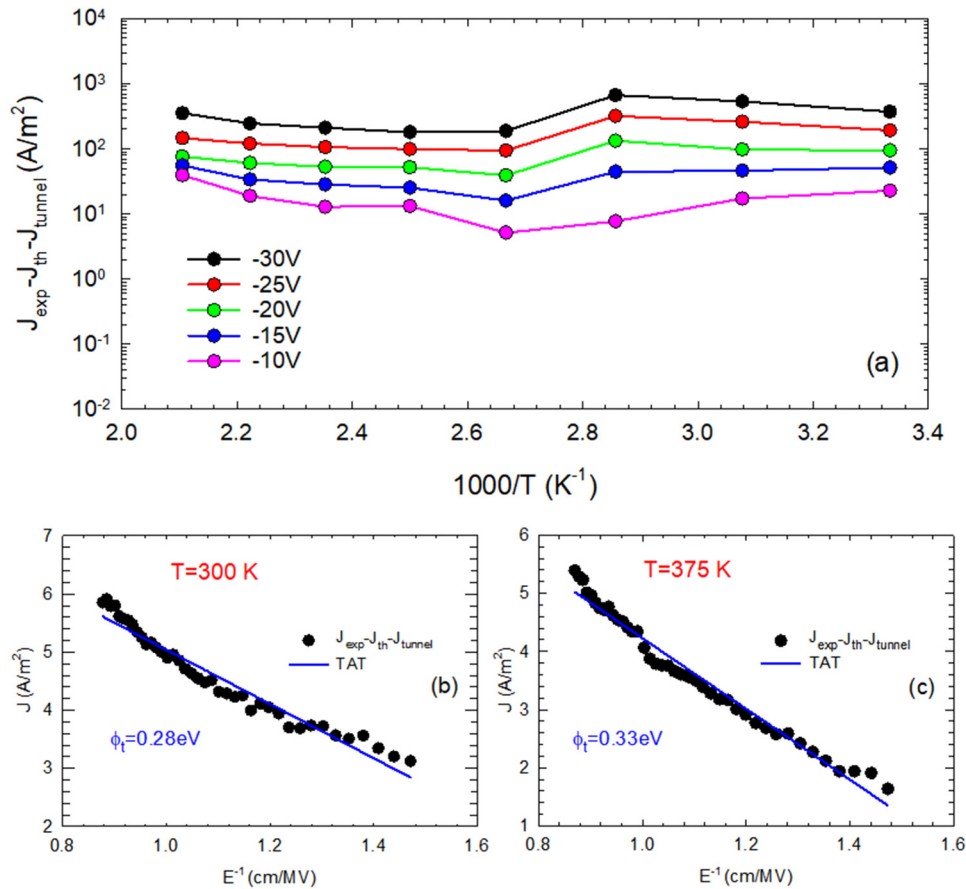


**FIG. 8.** (a) Reverse current density in excess of the ideal contributions as a function of  $1/T$  (from  $T=300$  to  $T=475$  K) for different values of reverse-bias voltage. Fitting of the results using the trap-assisted tunneling (TAT) model for (b)  $T=300$  K and (c)  $T=375$  K.

obtained from our model. For intermediate electric fields, our model matches with the Murphy and Good's thermionic field emission current ( $J_{\text{TFE}}^{\text{M-G}}$ ). Finally, for the higher electric fields, when electron injection takes place mainly near the metal Fermi level, our model fits accurately the analytical field emission current ( $J_{\text{FE}}^{\text{M-G}}$ ). As observed, the lower the temperature, the lower the electric fields at which TFE and FE become dominant.

To confirm that tunnel injection takes place at the expected energy regions when good agreement between our model and that of Murphy and Good is achieved, Fig. 7 shows the injected current as a function of energy at  $T=300$  K for surface electric fields of 0.20, 0.75, and 2.25 MV/cm, corresponding to the ranges of agreement with TE, TFE, and FE currents, respectively. As observed, for 0.20 MV/cm, even if having some tunnel injection, the main current contribution is thermionic emission over the barrier, as expected in the TE regime; for 0.75 MV/cm, tunneling is already dominant and injection occurs not far from the top of the barrier, as corresponds to the TFE regime; and for 2.25 MV/cm, it is localized around the Fermi level, as happens in the FE regime.

Once the model has been validated, it allows us to estimate the ideal leakage current due to thermionic emission and tunneling. Measured reverse current in excess of this ideal value indicates the presence of other leakage-current mechanisms, as happens in

Fig. 3(b) for temperatures below 425 K. Figure 8(a) represents the experimental values of the current subtracting the two ideal contributions to the leakage current estimated by the model for different temperatures (in the range of 300–475 K) and reverse-bias conditions (from  $-10$  to  $-30$  V). The excess current, while increasing with the reverse bias, does not change significantly with the temperature, thus allowing us to discard Poole-Frenkel emission and variable-range hopping mechanisms.<sup>20</sup> By representing this extra leakage current as a function of the inverse of the surface electric field for two different temperatures, 300 and 375 K [Figs. 8(b) and 8(c), respectively], a quasi-linear dependence is identified. This dependence indicates that the mechanism leading to the extra leakage current could be tunneling assisted by traps.<sup>20</sup> From the slope of the dependence, energies of the trap level in the range of 0.26–0.35 eV are identified (in particular, 0.28 and 0.33 eV for 300 and 375 K, respectively).

## V. CONCLUSIONS

A unified model for the calculation of ideal thermionic emission and tunneling currents in SBDs, including IC and doping effects, has been developed. The model addresses forward and reverse bias with the same set of physical parameters. Non-ideal



effects related to the series resistance and the ideality factor are included in the thermionic emission current in order to achieve a good fitting of the forward-bias experimental curves. The values of the barrier height, series resistance, and ideality factor are determined from such a fitting. The other parameters are the doping of the epilayer, calculated from the  $C$ - $V$  curves, and the dielectric constant and the effective mass of the semiconductor, taken from the literature. Once the parameters are known, they are used to predict the diode behavior in the reverse bias.

The model has been validated by comparison with current-voltage-temperature measurements performed in circular large-area GaN-on-SiC SBDs. An excellent fitting of the forward-bias  $I$ - $V$  curves has been achieved in a wide range of temperatures (275–475 K). In reverse bias, at the highest temperatures, the current is quite close to the ideal value predicted by the model, but at temperatures lower than 425 K, a significant deviation from the ideal behavior has been found and identified to be possibly due to trap-assisted tunneling.

Apart from the determination of the characteristic parameters of the SBDs, the model allows assessing how ideal is the behavior of SBDs in the reverse bias and which are the limits associated with a given technology. For example, it is possible to determine which is the voltage at which the ideal reverse leakage current reaches a given value limiting practical applications. It is also useful to evaluate the current in excess over the ideal value present in measurements in order to identify the leakage mechanisms at its origin, as done in the GaN diodes measured in this work.

## ACKNOWLEDGMENTS

This work has been partially supported through Grant No. PID2020-115842RB-I00 funded by No. MCIN/AEI/10.13039/501100011033. B. Orfao acknowledges the Ph.D. contract from the Junta de Castilla y León. This work was also supported by the French ANR (Agence National de la Recherche) through the project SchoGaN (No. ANR-17-CE24-0034), the “Investissements d’Avenir” program GaNeX (No. ANR-11-LABX-0014), and the French network Renatech.

## AUTHOR DECLARATIONS

### Conflict of Interest

The authors have no conflicts to disclose.

### Author Contributions

**B. Orfao:** Conceptualization (equal); Formal analysis (lead); Investigation (equal); Methodology (lead); Software (equal); Validation (lead); Writing – original draft (equal); Writing – review and editing (equal). **G. Di Gioia:** Resources (lead); Writing – review and editing (equal). **B. G. Vasallo:** Conceptualization (equal); Formal analysis (supporting); Investigation (equal); Methodology (supporting); Supervision (supporting); Validation (supporting); Writing – original draft (equal); Writing – review and editing (equal). **S. Pérez:** Conceptualization (equal); Formal analysis (supporting); Investigation (equal); Methodology (supporting); Supervision (supporting); Validation (supporting); Writing – original draft (equal); Writing – review and editing (equal).

**J. Mateos:** Conceptualization (equal); Formal analysis (supporting); Investigation (equal); Methodology (supporting); Supervision (equal); Validation (supporting); Writing – original draft (equal); Writing – review and editing (equal). **Y. Roelens:** Resources (lead); Writing – review and editing (equal). **E. Frayssinet:** Resources (lead); Writing – review and editing (equal). **Y. Cordier:** Resources (lead); Writing – review and editing (equal). **M. Zaknoute:** Resources (lead); Writing – review and editing (equal). **T. González:** Conceptualization (equal); Formal analysis (equal); Investigation (equal); Methodology (equal); Software (lead); Supervision (lead); Validation (equal); Writing – original draft (equal); Writing – review and editing (equal).

## DATA AVAILABILITY

The data that support the findings of this study are available within the article.

## REFERENCES

- <sup>1</sup>T. W. Crowe, J. L. Hesler, E. Bryerton, and S. A. Retzliff, in *Proceedings of the IEEE Compound Semiconductor Integrated Circuit Symposium (CSICS)* (IEEE, 2016), pp. 1–4.
- <sup>2</sup>A. Semenov, O. Cojocari, H.-W. Hübers, F. Song, A. Klushin, and A.-S. Müller, *IEEE Electron Device Lett.* **31**, 674 (2010).
- <sup>3</sup>F. Rettich, N. Vieweg, O. Cojocari, and A. Deninger, *J. Infrared Millimeter Terahertz Waves* **36**, 607 (2015).
- <sup>4</sup>A. S. Abdelrahman, Z. Erdem, Y. Attia, and M. Z. Youssef, *Can. J. Electr. Comput. Eng.* **41**, 45 (2018).
- <sup>5</sup>A. Ali, J. Chuanwen, Z. Yan, S. Habib, and M. M. Khan, *Energy Rep.* **7**, 5059 (2021).
- <sup>6</sup>H. Amano, Y. Baines, E. Beam, M. Borga, T. Bouchet, P. R. Chalker, M. Charles, K. J. Chen, N. Chowdhury, R. Chu *et al.*, *J. Phys. D: Appl. Phys.* **51**, 163001 (2018).
- <sup>7</sup>K. Hoo Teo, Y. Zhang, N. Chowdhury, S. Rakheja, R. Ma, Q. Xie, E. Yagyu, K. Yamanaka, K. Li, and T. Palacios, *J. Appl. Phys.* **130**, 160902 (2021).
- <sup>8</sup>K. Dang, J. Zhang, H. Zhou, S. Huang, T. Zhang, Z. Bian, Y. Zhang, X. Wang, S. Zhao, K. Wei, and Y. Hao, *IEEE Trans. Power Electron.* **35**, 2247 (2020).
- <sup>9</sup>I. Mehdi, J. V. Siles, C. Lee, and E. Schlecht, *Proc. IEEE* **105**, 990 (2017).
- <sup>10</sup>M. A. Ebrish, T. J. Anderson, A. D. Koehler, G. M. Foster, J. C. Gallagher, R. J. Kaplar, B. P. Gunning, and K. D. Hobart, *IEEE Trans. Semicond. Manuf.* **33**, 546 (2020).
- <sup>11</sup>S. M. Sze and K. K. Ng, *Physics of Semiconductor Devices* (John Wiley & Sons, New Jersey, 2007).
- <sup>12</sup>K. Ejderha, S. Duman, C. Nuhoglu, F. Urhan, and A. Turut, *J. Appl. Phys.* **116**, 234503 (2014).
- <sup>13</sup>M. Gülnahar, *Superlattices Microstruct.* **76**, 394 (2014).
- <sup>14</sup>W. Filali, N. Sengouga, S. Oussalah, R. H. Mari, D. Jameel, N. A. Al Saqri, M. Aziz, D. Taylor, and M. Henini, *Superlattices Microstruct.* **111**, 1010 (2017).
- <sup>15</sup>X. Guo, Y. Zhong, X. Chen, Y. Zhou, S. Su, S. Yan, J. Liu, X. Sun, Q. Sun, and H. Yang, *Appl. Phys. Lett.* **118**, 243501 (2021).
- <sup>16</sup>E. L. Murphy and R. H. Good, Jr., *Phys. Rev.* **102**, 1464 (1956).
- <sup>17</sup>F. A. Padovani and R. Stratton, *Solid State Electron.* **9**, 695 (1966).
- <sup>18</sup>J. Nicholls, S. Dimitrijević, P. Tanner, and J. Han, *Sci. Rep.* **9**, 3754 (2019).
- <sup>19</sup>W. Li, D. Jena, and H. G. Xing, *J. Appl. Phys.* **131**, 015702 (2022).
- <sup>20</sup>K. Fu, H. Fu, X. Huang, T. Yang, C. Cheng, P. R. Peri, H. Chen, J. Montes, C. Yang, J. Zhou, X. Deng, X. Qi, D. J. Smith, S. M. Goodnick, and Y. Zhao, *IEEE J. Electron Devices Soc.* **8**, 74 (2020).
- <sup>21</sup>J. Chen, Z. Liu, H. Wang, X. Song, Z. Bian, X. Duan, S. Zhao, J. Ning, J. Zhang, and Y. Hao, *Appl. Phys. Express* **14**, 104002 (2021).

- <sup>22</sup>G. Greco, P. Fiorenza, M. Spera, F. Giannazzo, and F. Roccaforte, *J. Appl. Phys.* **129**, 234501 (2021).
- <sup>23</sup>X. Kang, Y. Sun, Y. Zheng, K. Wei, H. Wu, Y. Zhao, X. Liu, and G. Zhang, *IEEE Trans. Electron Dev.* **68**, 1369 (2021).
- <sup>24</sup>K. Kim, D. Liu, J. Gong, and Z. Ma, *IEEE Electron Device Lett.* **40**, 1796 (2019).
- <sup>25</sup>X. Guo, Y. Zhong, Y. Zhou, S. Su, X. Chen, S. Yan, J. Liu, X. Sun, Q. Sun, and H. Yang, *IEEE Trans. Electron Devices* **68**, 5682 (2021).
- <sup>26</sup>M. Vivona, G. Greco, G. Bellocchi, L. Zumbo, S. Di Franco, M. Saggio, S. Rascunà, and F. Roccaforte, *J. Appl. Phys.* **54**, 055101 (2021).
- <sup>27</sup>G. di Gioia, “Gan Schottky diodes for THz generation,” Ph.D. thesis (Université de Lille, 2021).
- <sup>28</sup>W. Li, D. Saraswat, Y. Long, K. Nomoto, D. Jena, and H. G. Xing, *Appl. Phys. Lett.* **116**, 192101 (2020).
- <sup>29</sup>M. Hara, H. Tanaka, M. Kaneko, and T. Kimoto, *Appl. Phys. Lett.* **120**, 172103 (2022).
- <sup>30</sup>R. Fowler and E. A. Guggenheim, *Statistical Thermodynamics* (Cambridge University Press, New York, 1952), p. 460.
- <sup>31</sup>N. F. Mott and N. Sneddon, *Wave Mechanics and Its Applications* (University Press, Oxford, 1948), p. 23.
- <sup>32</sup>W. Götz, N. M. Johnson, C. Chen, H. Liu, C. Kuo, and W. Imler, *Appl. Phys. Lett.* **68**, 3144 (1996).
- <sup>33</sup>T. Maeda, M. Okada, M. Ueno, Y. Yamamoto, T. Kimoto, M. Horita, and J. Suda, *Appl. Phys. Express* **10**, 051002 (2017).